

End-to-end AI Framework for Interpretable Prediction of Molecular and Crystal Properties

Hyun Park^{1,3,7}, Ruijie Zhu^{2,3}, E. A. Huerta^{3,4,5}, Santanu Chaudhuri^{3,6}, Emad Tajkhorshid^{1,7,8} and Donny Cooper⁹

¹ Theoretical and Computational Biophysics Group, Beckman Institute for Advanced Science and Technology, University of Illinois at Urbana-Champaign, Urbana, Illinois 61801, USA

² Department of Materials Science and Engineering, Northwestern University, Evanston, Illinois 60208, USA

³ Data Science and Learning Division, Argonne National Laboratory, Lemont, Illinois 60439, USA

⁴ Department of Computer Science, University of Chicago, Chicago, Illinois 60637, USA

⁵ Department of Physics, University of Illinois at Urbana-Champaign, Urbana, Illinois 61801, USA

⁶ Multiscale Materials and Manufacturing Lab, University of Illinois Chicago, Chicago, Illinois 60607, USA

⁷ Department of Biochemistry, University of Illinois at Urbana-Champaign, Urbana, Illinois 61801, USA

⁸ Center for Biophysics and Quantitative Biology, University of Illinois at Urbana-Champaign, Urbana, Illinois 61801, USA

⁹ Computational Science and Engineering, Data Science and AI Department, TotalEnergies EP Research & Technology USA, LLC, Houston, Texas 77002 USA

E-mail: hyunp2@illinois.edu

December 2022

Abstract. We introduce an end-to-end computational framework that allows for hyperparameter optimization using the `DeepHyper` library, accelerated model training, and for interpretable AI inference. The framework is based on state-of-the-art AI models including `CGCNN`, `PhysNet`, `SchNet`, `MPNN`, `MPNN-transformer`, and `TorchMD-NET`. We employ these AI models along with the benchmark `QM9`, `hMOF`, and `MD17` datasets to showcase how the model can predict user-specified material properties within modern computing environments. We demonstrate translational applications in the modeling of small molecules, inorganic crystals and nanoporous metal organic frameworks with a unified, standalone framework. We have deployed and tested this framework in the ThetaGPU supercomputer at the Argonne Leadership Computing Facility (ALCF), and in the Delta supercomputer at the National Center for Supercomputing Applications (NCSA) to provide researchers with modern tools to conduct accelerated AI-driven discovery in leadership-class computing environments.

Keywords: AI, Molecules, Crystals, Metal-Organic Systems, Interpretable AI

1. Introduction

With the explosion of AI models [1, 2, 3, 4, 5] developed to predict various material properties over the recent years, it has become difficult to keep track of the available AI models and the datasets that are used for training and inference. Numerous efforts [6, 7] have been made toward the integration of AI models and their associated datasets in one place to streamline their use for a wide range of applications and a broad community of users [8, 9, 10]. AI models and datasets are often available through open repositories, in the best scenario, so a user can download, deploy and reproduce their putative capabilities. Unfortunately, this is a time-consuming and laborious process, which can be further complicated when tools and libraries used to develop the AI models are not available, deprecated, or non-backwards compatible in computing environments of new users. Furthermore, most of the existing packages are specialized in predicting quantum mechanical (QM) properties of small molecules, few of them support crystals.

In order to address these shortcomings, here we report the construction of a computational framework that consolidates libraries, AI models and AI interpretability tools to study molecules, crystals, and metal-organic frameworks. The framework enables hyperparameter tuning through the open source library DeepHyper [11], model training, and interpretable inference of small-molecule QM properties from public datasets such as QM9 [12], and crystal properties from datasets such as hMOF [13].

Key aspects of this computational framework include:

Novel features of AI models. The node and edge embedding schemes of two graph neural network models, PhysNet and CGCNN, were modified from the original adjacency matrix format to an adjacency list format to reduce redundant information and enable faster training. We also adapted small-molecule property prediction models to take in crystal structures as input such as the crystal version of SchNet.

Translational AI applications. We demonstrate the transferability of the learned force fields by training TorchMD-NET model using selected molecular dynamics (MD) trajectory data of a given set of molecules in the MD17 dataset [14] to perform MD simulations of similar molecules. In particular, we show that a model trained based on ethanol is transferable to both *n*-propanol and iso-propanol, and a model trained using uracil is transferable to pyrimidine and naphthalene. All of the results are automatically logged to weights and biases (WandB) [15], a machine learning tracking tool, for simple access.

Interpretable AI inference. To gain a better understanding of the model predictions, we provide two novel functionalities to explain the learned features. First, by mapping the last hidden layer of the model onto a 3D plane via the UMAP method, we can make more sense of the molecular clusters with similar properties. Second, by highlighting selected atoms of molecules via the Grad-CAM method, we can now identify which atoms are significant for model predictions.

We expect that this collection of state-of-the-art graph neural networks, transformer models, and analysis methods for small molecules, crystals and metal-organic-frameworks will empower AI practitioners to seamlessly perform hyperparameter optimization, accelerated training and inference, and interpretable AI in modern computing environments with a unified, standalone computational framework.

2. Related work

Graph neural networks have shown great success for modeling molecular and crystal structures. For small molecules, a suite of models have been proposed, including DimeNet [4], GemNet [16], SchNet [1] and PhysNet [2]. These models take in atomic coordinates and atomic numbers as input, and represent atoms as nodes and bonds as edges. Typical target properties for these models are QM molecular properties such as internal energy, heat capacity and zero point vibrational energy. For crystal structures, periodic boundary conditions need to be considered, therefore crystal graph representations are typically used. Example graph neural networks that take in crystal structures as input include ALIGNN [17], CGCNN [5], and MEGNet [18]. These models first extract crystal graphs from the structures, then generate atomic and edge embeddings for the center atoms and their neighbors. The bond and edge information is then updated via message passing. The target properties for these models are similarly QM properties of crystals, e.g., formation energy and band gap.

The growing number of the graph neural networks available for this purpose pushes the need for an end-to-end AI framework. Previous efforts toward such a goal typically missed one or more important aspects. For example, MatDeepLearn [7] integrates a suite of graph neural networks, including CGCNN, MEGNet, MPNN, GCN and SchNet. Although it can be used for hyperparameter tuning, model training, and inference, it lacks the explainability feature, which limits the amount of chemical insights that could be extracted from the results. Another example is Dive in Graphs (DIG) [6], which enables model training and explanation. However, it does not allow for hyperparameter tuning, therefore only models with preset hyperparameters can be used. A complete package offering all of the aforementioned functionalities is therefore needed.

Our AI framework also offers the functionality to perform molecular dynamics for small molecules, enabled by TorchMD-NET [3], an SE3-equivariant transformer interatomic potential model that establishes a relationship between atomic configurations and potential energies and forces. The MD trajectories of selected molecules taken from the MD17 dataset were used for training the TorchMD-NET models.

3. Methods

Here we describe the key building blocks of our general-purpose AI framework:

- (i) It provides built-in datasets and neural networks that we modified to take in adjacency list format node and edge embeddings, a more efficient embedding scheme

than adjacency matrix format

- (ii) It enables distributed hyperparameter tuning of neural networks via the scalable and computationally efficient library `DeepHyper`
- (iii) Model training and interpretable inference are performed by specifying a few command line arguments
- (iv) Results are auto-logged to `WandB`, a machine learning tool for easy tracking and visualization
- (v) MD simulations can be performed for small molecules using `TorchMD-NET` if trained with MD trajectories from the MD17 dataset, enabled by the atomic simulation environment (ASE) library [19].

This framework has been deployed and tested in leadership computing platforms to reduce the overhead for researchers that require access to hyperparameter tuning, model training and explainable inference tools in a single, unified framework. Below we describe each of these components in further detail.

Hyperparameter tuning. This feature was done using the `DeepHyper` [11] library. In this method, hyperparameters of interest are given prior distributions and their posterior distributions are adjusted based on the Centralized Bayesian Optimization (CBO) algorithm with a given acquisition function and a surrogate model. The graph neural networks in this framework are coupled with `DeepHyper` to enable faster hyperparameter tuning.

Datasets QM9 and MD17 datasets were used as input to graph neural networks. The QM9 dataset consists of molecular structures and QM properties of 133,885 molecules with up to nine atoms of type H, C, O, N and F. For demonstration purposes, the selected QM properties in this work include the highest occupied molecular orbital (HOMO), and zero point vibrational energy (ZPVE). The MD17 dataset consists of ab-initio MD trajectories of 10 molecules at different levels of theory. Both datasets are available in the `PyTorch Geometric` library.

Node and edge embedding schemes. Instead of using the original adjacency matrix format for node and edge embeddings, we modified them to adjacency list format. The term embedding, for both molecular and crystal graphs, refers to the information attached to a node (an atom) or an edge (a bond). Both node and edge embeddings can be scalars, vectors or higher order tensors. The node embeddings encode information such as mass, charge and orbital hybridization, whereas the edge embeddings encode information such as interatomic distance and bond order. Depending on the model architecture, some embeddings are physics or chemistry based while others are learned. For physics- or chemistry-based embeddings, the information such as hybridization, mass, atomic radius, and whether the fragment is a part of an aromatic ring is encoded. On the other hand, learned embeddings refer to the embeddings that are optimized by a neural network model via stochastic gradient descent.

In adjacency matrix format edge embeddings, the adjacency matrix is encoded into a fixed-size matrix, whose size is determined by the largest molecule in the dataset. For other molecules, their vectors are padded to be the same dimension as the largest one. Each element in the adjacency matrix indicates whether the two corresponding nodes are connected, as determined via some distance-based criteria. Since padding is applied to smaller molecules in the matrix, users need to know a priori the largest molecule size, then perform masking to obtain the padding values, which can be burdensome for GPU memories. By using the adjacency list format, however, only the information for connected atoms is preserved, thereby avoiding the need for padding and taking less memory to load. In this case, faster model training and inference loss convergence speed and higher accuracy are expected. The adjacency list format has been implemented in a number of Python libraries such as Deep Graph Library (DGL) [20] and PyTorch Geometric [21]. We will use the CGCNN model as an example to demonstrate a boost in model training performance when an adjacency list format is used in place of an adjacency matrix format.

Our AI framework allows users to perform hyperparameter tuning, model training and interpretable inference for pre-trained models or train new models with a few arguments passed. The main improvements over previous general-purpose machine learning model training libraries is the explainability feature, which consists of two parts. First, by extracting high dimensional hidden layer information from the learned models and projecting it onto low dimensions via the uniform manifold approximation and projection (UMAP) technique, we can effectively visualize the clustering of molecules, with similar practice as in [22, 23, 24]. Second, Saliency, CAM and Grad-CAM methods are used to highlight important atoms in molecular graphs, as described in [25].

4. Results

Below we present a comprehensive analysis of our results, from hyperparameter optimization to interpretable AI inference.

4.1. Hyperparameter Optimization

The DeepHyper library was used for hyperparameter tuning of graph neural networks. DeepHyper is easy to use and can be readily deployed on GPU-based high-performance computing platforms. CPUs can be used if GPUs are not available. However, if the user has access to multiple GPUs, then the GPU option will be automatically chosen, with each core performing hyperparameter search using the CBO algorithm, given an acquisition function such as the upper confidence bound, and a surrogate model, e.g., random forest.

The list of hyperparameters considered in this work along with their ranges are summarized in Table 1. Hyperparameter tuning results for PhysNet with ZPVE as target property are shown in Tables 2 and 3. It is worth mentioning that since DeepHyper tries

to maximize the objective of search, the opposite number of validation error was used as the objective, therefore a larger absolute value of objective corresponds to a better combination of hyperparameters. The hyperparameter tuning results for PhysNet with HOMO as the target property are shown in Tables A1 and A2

Table 1. List of hyperparameters and their ranges.

hyperparameter	log scale	range
<code>agb</code>	true	[1,20]
<code>amp</code>	false	[true,false]
<code>batch size</code>	/	[128,512]
<code>epochs</code>	true	[10,100]
<code>gradient clip</code>	true	[1e-05,2]
<code>learning rate</code>	true	[1e-3,1]
<code>optimizer</code>	/	[SGD,TorchAdam,Adam,LAMB]
<code>weight decay</code>	true	[2e-6,0.02]

Among the hyperparameters, `agb`—accumulated grad batches—helps overcome memory constraints; `amp`—automatic mixed precision— speeds up neural network training; and `gradient clip`, a machine learning technique where the gradient of neural network parameters is re-scaled by a coefficient between 0 and 1, is known to stabilize neural network training by avoiding sudden changes in parameter values (also known as exploding gradient problem) [26].

Table 2. Top 10 DeepHyper hyperparameter combinations for PhysNet with ZPVE as target property.

	<code>agb</code>	<code>amp</code>	<code>batch_size</code>	<code>gradient_clip</code>
4	TRUE		190	0.00245
3	TRUE		190	0.00022
1	TRUE		397	0.00032
4	TRUE		196	0.00122
3	TRUE		174	1.60E-05
4	TRUE		154	3.25E-05
4	TRUE		300	0.732
4	TRUE		228	0.00389
2	FALSE		359	0.72537
11	TRUE		168	0.00243

The optimal hyperparameter combinations found by DeepHyper are listed in the top rows of Tables 2 and 3. The optimal objective is -0.9226. We notice that the optimal hyperparameters include f32 precision (`amp="false"`), a standard learning rate (0.00296), and a low gradient norm clipping value (0.00245). These result in small gradient accumulation, which may help mitigate sudden gradient updates.

Table 3. As Table 2 for the rest of parameters optimized through DeepHyper.

learning_rate	optimizer	weight_decay	objective
0.00296	torch_adam	1.03E-05	-0.9226
0.75169	torch_adam	5.14E-06	-6.7526
0.00015	lamb	2.69E-06	-6.7925
0.32274	lamb	1.45E-05	-7.1168
0.17673	lamb	7.80E-06	-12.31
0.00144	torch_adam	1.13E-05	-15.394
0.02986	lamb	3.57E-06	-26.13
0.00966	torch_adam	7.16E-06	-27.627
0.02491	sgd	1.04E-05	-29.335
0.00124	torch_adamw	0.00011	-30.203

We have tested multiple sets of hyperparameters with varying ranges and prior distributions. Our hyperparameter tuning configuration input file is prepared in `YAML` format. Discrete hyperparameter values such as the number of epochs and the batch size are sampled from uniform distributions whereas continuous hyperparameters such as the learning rate and the gradient clip are sampled from normal distributions with/without log scale. The ranges of hyperparameters along with the prior distributions for sampling are both user-customizable.

Once the hyperparameter configuration and the prior distributions are in place, `DeepHyper` can use multiple GPUs to perform hyperparameter tuning, taking full advantage of GPU parallelization. Next, all the optimization results will be saved and automatically logged to `Weights and Biases`. If the tuning step is interrupted, it can be resumed from the last saved checkpoint by specifying the `--resume` tag.

For the `PhysNet` model with `HOMO` and `ZPVE` as target properties, we compared hyperparameter tuning performance of `DeepHyper` with a naive algorithm that performs random selection of hyperparameters. Since `DeepHyper` utilizes the `CBO` algorithm to optimize hyperparameters, the target property values are used for decision making. For the naive algorithm, however, hyperparameters were randomly selected from the hyperparameter grid in Table 1. A total of 20 models were trained for 30 epochs with hyperparameters given by the two methods. The distributions of the losses (means squared error) are compared in Figure 1, and the metrics are summarized in Table 4.

Key findings: For the prediction of `HOMO` and `ZPVE`, `DeepHyper` yields better hyperparameter combinations, which accelerate convergence and provide optimal performance.

4.2. AI model training

We trained `PhysNet`, `SchNet`, `MPNN` and `MPNN-transformer` (with attention mechanism) with `HOMO` and `ZPVE` as target properties from the `QM9` dataset. The models were trained

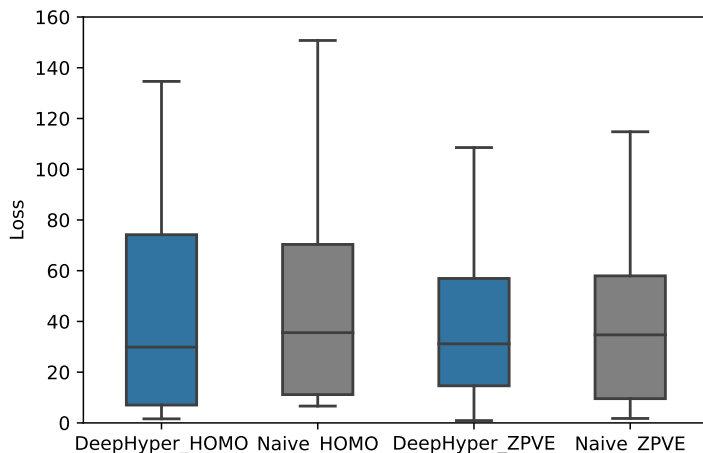


Figure 1. Comparison of the loss distributions of PhysNet with hyperparameters found by DeepHyper (blue) and a naive random selection algorithm (grey). Two outliers for the DeepHyper_HOMO box were neglected to retain details.

Table 4. Performance of 20 models with hyperparameters found by DeepHyper and a naive random selection algorithm with HOMO and ZPVE as target properties. For both properties, the minimum loss and the standard deviation of loss are reported.

	HOMO		ZPVE	
	min_loss	std_loss	min_loss	std_loss
DeepHyper	1.604	74.871	0.923	31.771
Naive Algorithm	6.632	52.43	1.751	65.117

for 1,500 epochs to ensure convergence of validation loss. A new model is saved when the validation loss drops. The model training results are summarized in Figure 2. We found that ZPVE is an easier property to learn compared to HOMO for all four models, as indicated by a significantly lower loss. Moreover, the addition of attention layer in the MPNN model (MPNN-transformer) further lowers the mean absolute error (0.09 eV for HOMO and 0.01 eV for ZPVE) compared to the original MPNN model (0.15 eV for HOMO and 0.03 eV for ZPVE).

Model uncertainty quantification was performed for PhysNet model with HOMO and ZPVE as target properties. Five PhysNet models with randomly initialized weights were generated using the random seeds method. The optimal hyperparameter combinations found by DeepHyper in Section 4.1 were used. The models were trained for 100 epochs to achieve convergence of loss function. Figure 3 shows that PhysNet makes consistent predictions regardless of the random initial weights. The standard deviations of losses for the five models with HOMO and ZPVE as target properties are 0.0379 eV and 3.9646e-05 eV, respectively, and the mean absolute errors are comparable with those reported in the literature [27].

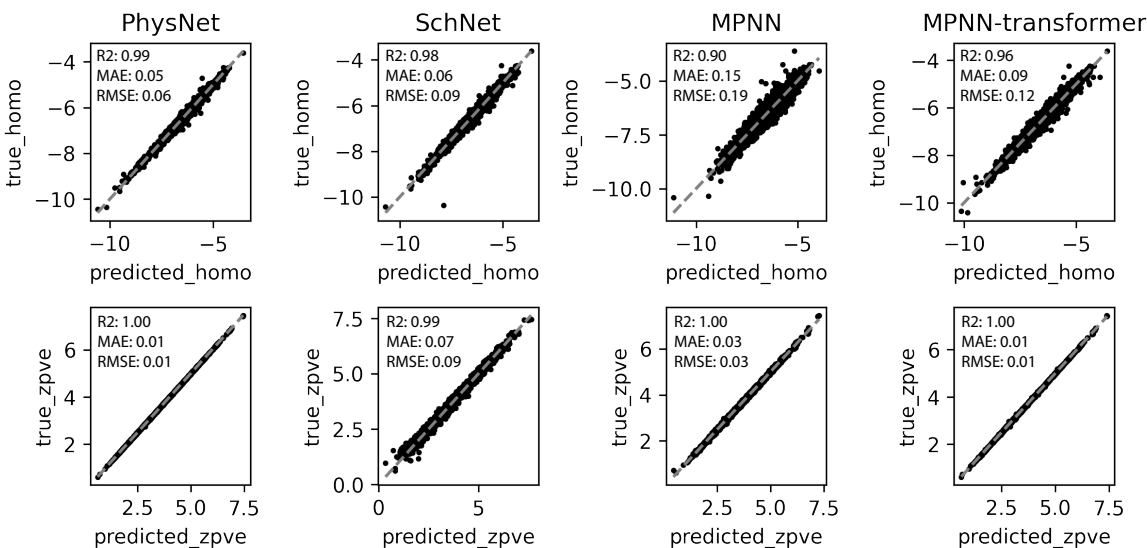


Figure 2. From left to right, model inference performance of PhysNet, SchNet, MPNN and MPNN-transformer with HOMO (top row) or ZPVE (bottom row) as the target property.

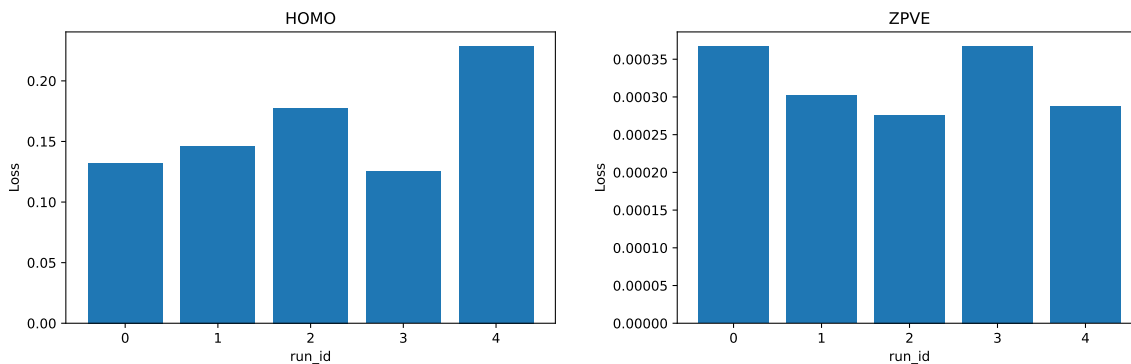


Figure 3. Model training performance of PhysNet with HOMO (left) and ZPVE (right) as target properties, initialized with 5 random seeds.

Key findings: Our suite of AI models provide state-of-the-art results. Novel features that we added to the models, such as attention to MPNN-transformer, further improve their performance. We have also demonstrated that hyperparameter optimization leads to stable, statistically robust AI predictions.

4.3. Model improvement via modified node and edge embedding schemes

We modified the node and edge embedding schemes of CGCNN model from the original adjacency matrix format to an adjacency list format. There are two main advantages in using the adjacency list format. First, compared to the adjacency matrix format, it takes up less memory for loading, which speeds up model training. Second, the redundant information (zero paddings) in the representation is removed, resulting in

higher training accuracy and stability. As an example, CGCNN models with the two embedding schemes were trained on a subset of the hMOF database [28], which contains 5,000 randomly selected MOF structures along with their CO₂ working capacities at 2.5 bar. The model training results are shown in left panel of Figure 4. To smooth out local fluctuations, thirty point moving averaging was performed on both curves. We notice that CGCNN model with adjacency list format node and edge embeddings achieved faster convergence speed, higher training stability, and a lower mean absolute error (MAE) compared to the original CGCNN model.

From the right panel of Figure 4, we show that the improved CGCNN model predicts CO₂ working capacity with a MAE of 0.32 mmol/g. To better understand the predictive performance of the improved CGCNN model, we benchmarked it against two recently proposed machine learning models for predicting CO₂ working capacity of MOFs, namely ALIGNN [29] and random forest regressor [30].

ALIGNN was trained on the entire hMOF dataset and predicts CO₂ working capacity at 2.5 bar with a MAE of 0.48 mmol/g, which is 50% higher loss value than our model. This could be because they trained the model on the entire hMOF dataset, whereas we randomly sampled around 5000 structures from the database for training. Note that ALIGNN uses both normal graph and line-graph (i.e. edges of normal graph are line-graph nodes while line-graph edges are interactions between line-graph nodes) for training and inference of working capacity prediction. For a normal graph, it uses physical and chemical features for atom (node) embedding, and distances between atoms as edge embedding; for a line graph, distances are line-graph node embedding while bond angle embedding is line-graph edge embedding. This scheme, however, can cause occasional CUDA memory issues and training batch size may have to be reduced (64 in [29]; 32 in our independent experiment), hence slower training. On the other hand our improved CGCNN model only takes in crystal structures as input (i.e. atom species and Cartesian coordinates) with larger batch size (256 in our model).

The random forest regression model takes in topological, structural, and word embeddings features as input. When trained on the entire hMOF dataset, it achieves an RMSE and R² score of roughly 0.65 and 0.95, respectively, for the prediction of CO₂ working capacity at 2.5 bar, which is 27% higher error value for RMSE than our model. Overall, the improved CGCNN model achieves competitive predictive performance compared to state-of-the-art machine learning models.

In other papers not using hMOF dataset and/or predicting other MOF properties, extensive physical and chemical featurizations were used [31][32], whereas our model learns the MOF information from only atom species and coordinates.

Key findings: Adopting adjacency list format node and edge embedding scheme improves the predictive capabilities of our improved CGCNN model. Using a test set of over 500 MOFs from the hMOF dataset, we have found that our improved CGCNN model provides state-of-the-art predictions for CO₂ working capacities at 2.5 bar.

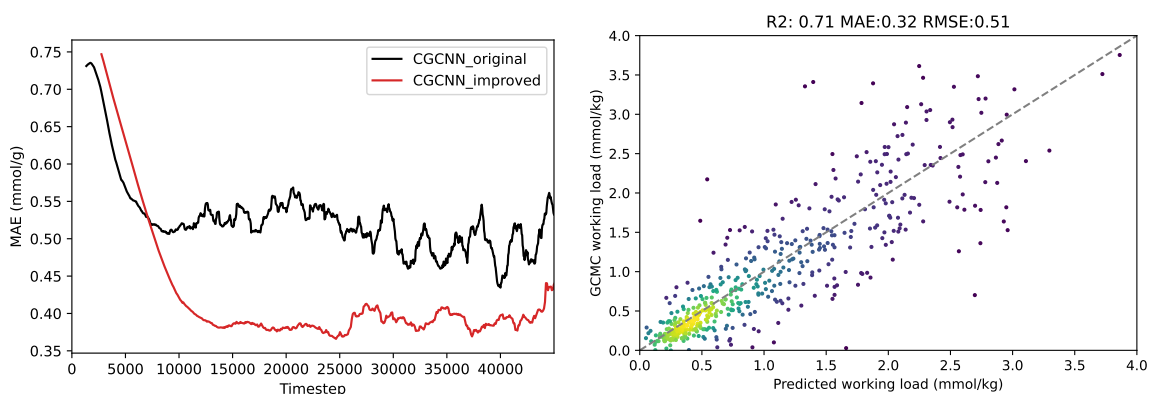


Figure 4. Left panel, comparison of the original CGCNN model (black) with adjacency matrix format node and edge embedding schemes and the modified CGCNN model (red) with adjacency list format node and edge embedding schemes. Right panel, predictive performance of our improved CGCNN model on a test set (10% of our sampled 5000 structures) of 522 MOFs of the hMOF dataset. The lower and upper bound of both axes were constrained to 0 mmol/g and 4 mmol/g to reflect the typical working capacity range.

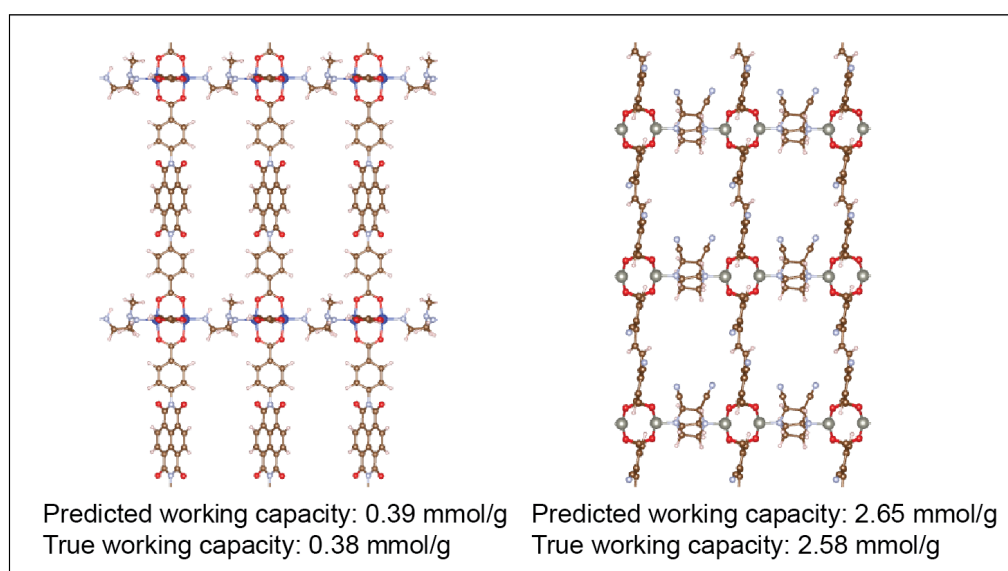


Figure 5. Sample MOF structures in the hMOF database along with the AI predicted and ground truth CO₂ working capacities at 2.5 bar.

4.4. Translational AI Applications

MD simulations of two sets of small molecules were performed to demonstrate the transferability of TorchMD-NET: from ethanol to *n*-propanol and *iso*-propanol and from uracil to pyrimidine and naphthalene.

In each set, the TorchMD-NET model trained with MD trajectories of the molecule on the left was used to perform MD simulations of the molecules on the right. The NVE ensemble was used, where the total number of particles and the simulation box volume is fixed and the total energy is conserved. For all molecules, the number of timesteps

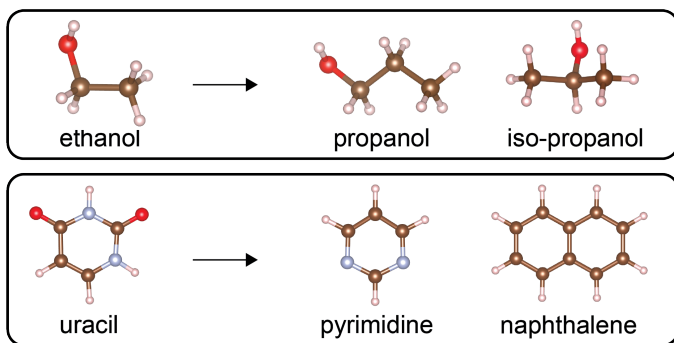


Figure 6. Example molecules used to demonstrate the transferability of TorchMD-NET. MD trajectories of molecules on the left are used to train the TorchMD-NET model, which is then used to perform MD simulations for the molecules on the right.

and the total simulation time were chosen to be 0.1 fs and 10 ps (100,000 timesteps), respectively. Figure 7 shows that the C-C and C-O bond length distributions of ethanol, *n*-propanol and *iso*-propanol have similar means, whereas the latter two have a larger spread. It is worth noting that for *n*-propanol, the length of the C-C bond closer to the O atom has a very similar distribution to that of ethanol, which is expected because their local environments are similar. For bond angles, The C-C-O bond angle distribution of ethanol exhibits two peaks, whereas the other two only have one peak. For uracil, pyrimidine and naphthalene, the C-C bond length distribution of naphthalene is shifted to a higher range compared to the other two, which may be due to the absence of N atoms in its ring structure. The C-N bond length distributions of uracil and pyrimidine have similar means, whereas the latter has a larger spread. Similarly, we observe comparable C-C-C bond angle distributions in uracil and pyrimidine, whereas the same distribution for naphthalene is shifted to a higher range, again an effect which may be due to the absence of N atoms in naphthalene’s ring structure. The similarity and differences of bond length and angle distributions demonstrate that TorchMD-NET trained on one type of molecule is transferable to other similar molecules.

Key findings: We present a novel application of TorchMD-NET, in which this AI model was fine-tuned to describe a given small molecule by accurately predicting its potential energy and forces and perform NVE MD simulations, and then seamlessly used to describe other molecules with different structures, while still capturing physically realistic bond length and angle distributions.

4.5. Interpretable Inference

Model performance attribution. By projecting the second last layer’s high dimensional vector representation of graph neural network onto molecular structure and visualizing the projection, we can better understand the physical and chemical properties of the input data that affect predictions of our AI models. The top panels of Figure 8 present model interpretation results of how PhysNet model predicts HOMO

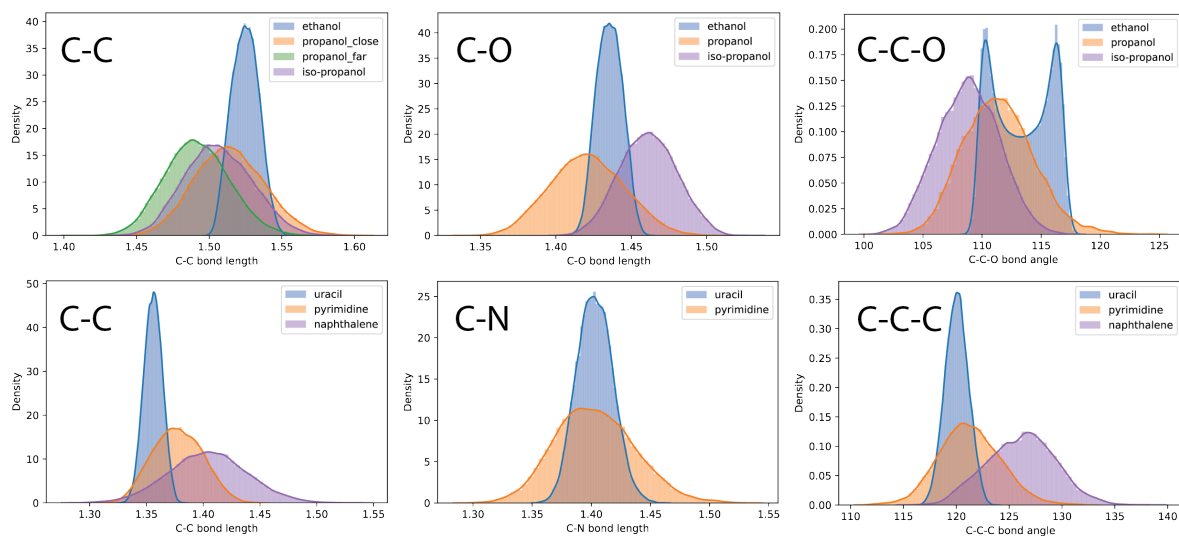


Figure 7. Top row, distributions of select bond lengths and angles in ethanol, *n*-propanol, and *iso*-propanol. Bottom row, distributions of select bond lengths and angles in uracil, pyrimidine, and naphthalene.

based on molecular structures via the Grad-CAM method. The N atoms and the H atoms connected to them are highlighted, possibly indicating that for PhysNet, these atoms carry more weight in the prediction of HOMO. We do not claim that explanations found by our deep learning model are the definite reasons for accurate prediction of QM properties such as HOMO or ZPVE, since these QM properties may not be simply determined by atomic species and coordinates. However, AI-explained visualization can help us better make sense of the patterns of complex molecular property predictions.

Dimension Reduction To reveal the correlation between model features and target properties, we applied uniform manifold approximation and projection (UMAP) dimension reduction technique to find the distribution of small molecules by projecting their high-dimensional structural/chemical data onto lower-dimension spaces. UMAP has been shown to achieve comparable or even better performance than other dimension reduction techniques such as principal component analysis (PCA) [33] and t-distributed stochastic neighbor embedding (tSNE) [34] on non-linear datasets [35]. Dimension reduction result for the PhysNet model with HOMO as target property is shown in the bottom panel of Figure 8, where each dot in the plot represents a molecule, color-coded based on its corresponding HOMO value. A 10% randomly selected subset (13.4k molecules) of the QM9 dataset was used to produce these results, which consists of stable small molecules composed of CHONF. From the scatter plot we know that molecules with similar HOMO values are clustered together and there is clear separation of molecules with low and high HOMO values. We present additional illustrative results in Appendix B.

Roughness of Molecular Property Landscape. For molecular property prediction,

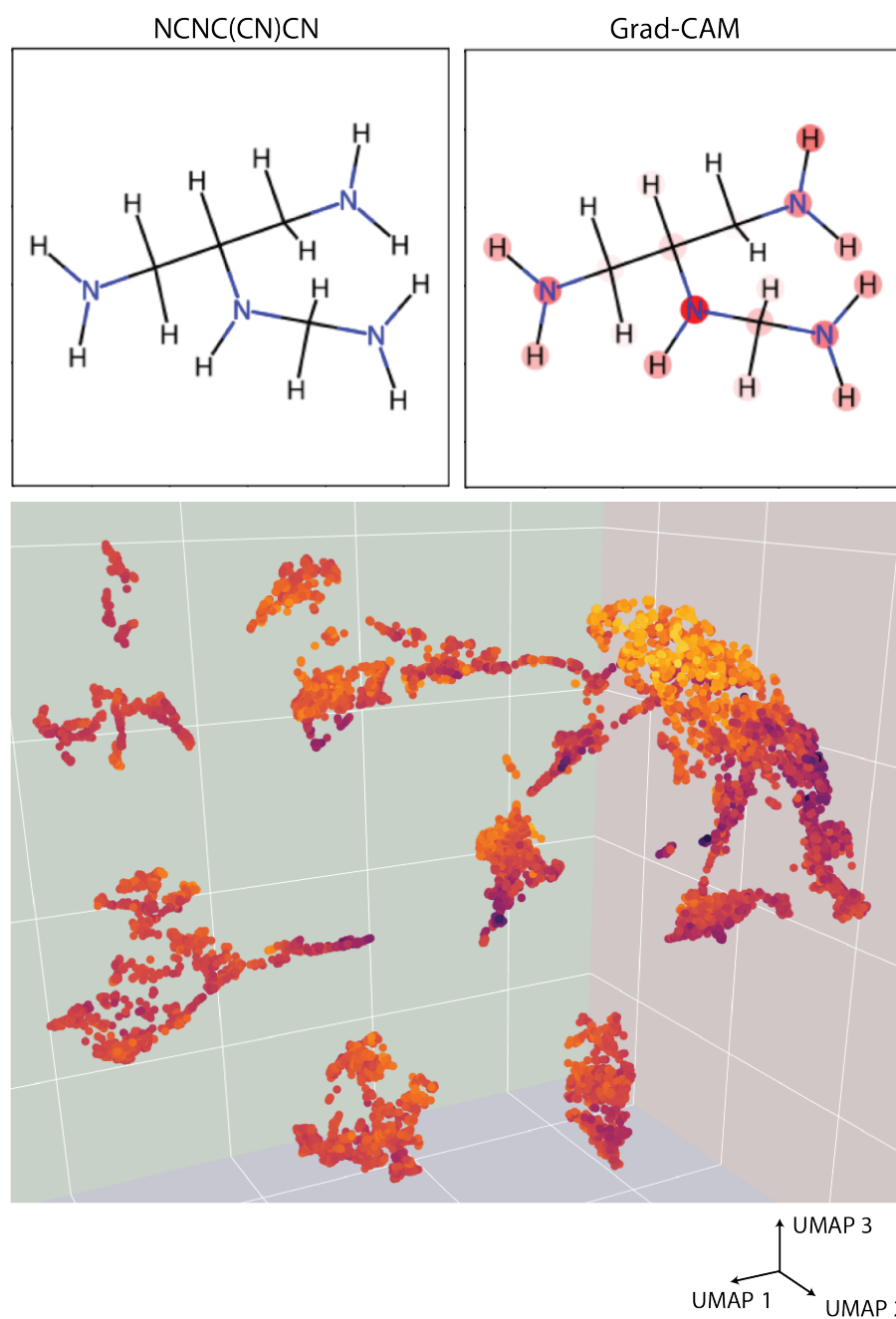


Figure 8. Top panels: exploration of the PhysNet model prediction using Grad-CAM method. Heavier atoms (N atoms) and the H atoms connected to them are highlighted in red, indicating their higher weight in HOMO prediction. Bottom panel: Uniform manifold approximation and projection (UMAP) dimension reduction results for the PhysNet model with HOMO as target property. Gold and purple dots represent molecules with high and low HOMO values, respectively.

the predictive performance of graph neural networks has shown to correlate to the roughness of molecular property landscape [36] [37] [38]. We adopted the recently proposed state-of-the-art roughness index (ROGI) [39] to measure how rough the HOMO and ZPVE landscapes are for PhysNet, SchNet, MPNN, MPNN-transformer. The calculation of molecular landscape roughness involves specifying a molecular representation and a distance metric. Molecular representations can be either learned by the graph neural network, with values extracted from the second last layer, or calculated based on molecular structures, as represented by SMILES strings or 3D Cartesian coordinates. The distance metrics are used to measure how different two molecular representations are. Example distance metrics include Tanimoto similarity, Euclidean distance, cityblock distance and cosine distance. To calculate ROGI values, learned molecular representation and one of the aforementioned distance metrics are used. Using Euclidean distance as the distance metric and HOMO as the target property, we show the ROGI values and mean absolute errors of four graph neural networks in Figure 9. We observe that a lower ROGI value in general corresponds to a lower mean absolute error, that is, higher predictive performance. We attribute this trend to the direct relation of a higher performing model to the smoothness of the resulting molecular property landscape. The exception is MPNN, which corresponds to a lower ROGI value despite a higher MAE as compared to the MPNN-transformer, which may be because the addition of transformer layers roughens the molecular property landscape while facilitating model training.

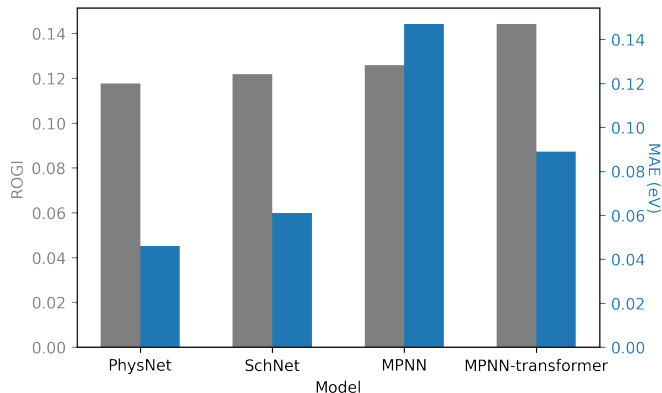


Figure 9. Roughness of the HOMO landscape (gray) and mean absolute error of model predictions (blue) for PhysNet, SchNet, MPNN and MPNN-transformer

Key findings: Our proposed approach brings together disparate interpretability AI tools to explore and make sense of AI model predictions, encompassing model performance attribution and scientific visualization; dimension reduction with UMAP to explore clustering of molecules with similar properties; and metrics such as the roughness index to quantify the predictive performance of our AI models for QM properties. These complementary tools provide valuable insights into the features and patterns of input data that are relevant for AI inference.

5. Conclusion

The rise of AI in the early 2010s was possible by a combination of elements, including disruptive technologies and computing approaches, as well as the desire to advance state-of-the-art practice through collaborative and friendly competitions in which high-quality datasets and AI models were freely shared. Similar approaches have been mirrored in science and engineering in recent years. These efforts are now being formalized through FAIR (findable, accessible, interoperable and reusable) initiatives [40, 41] in the context of scientific datasets [42], research software [43] and AI models [8, 44]. This study represents yet another significant step in this direction. We have assembled benchmark datasets, added novel features to state-of-the-art graph neural networks and transformer models, coupled them with robust libraries for hyperparameter tuning to improve their capabilities for scientific discovery, and developed and adapted a set of visualization and interpretability tools to make sense of the AI predictions. All these elements are unified within a single computational framework that has been deployed and extensively tested on leadership-class, high-performance computing platforms. Researchers using this computational framework will be able to conduct scientific discovery combining state-of-the-art AI models with datasets that are coupled with advanced supercomputing platforms. We expect that this approach will catalyze the sharing of AI knowledge and tools in the context of molecular and crystal property prediction applications.

6. Acknowledgments

This work was supported by the FAIR Data program and the Braid project of the U.S. Department of Energy, Office of Science, Advanced Scientific Computing Research, under contract number DE-AC02-06CH11357. It used resources of the Argonne Leadership Computing Facility, which is a DOE Office of Science User Facility supported under Contract DE-AC02-06CH11357. This work was supported by Laboratory Directed Research and Development (LDRD) funding from Argonne National Laboratory, provided by the Director, Office of Science, of the U.S. Department of Energy under Contract No. DE-AC02-06CH11357. This research used the Delta advanced computing and data resource which is supported by the National Science Foundation (award OAC 2005572) and the State of Illinois. Delta is a joint effort of the University of Illinois at Urbana-Champaign and its National Center for Supercomputing Applications. We thank Prasanna Balaprakash and the [DeepHyper](#) team for their expert support and guidance as we coupled their library into our computational AI framework.

Code availability

The AI models [PhysNet](#) [45] and [MPNN_transformer](#) [46] presented in this study are freely available at the Data and Learning Hub for Science [47, 48].

ORCID IDs

Santanu Chaudhuri [0000-0002-4328-2947](https://orcid.org/0000-0002-4328-2947)Eliu Huerta [0000-0002-9682-3604](https://orcid.org/0000-0002-9682-3604)Hyun Park [0000-0001-5550-5610](https://orcid.org/0000-0001-5550-5610)Emad Tajkhorshid [0000-0001-8434-1010](https://orcid.org/0000-0001-8434-1010)Ruijie Zhu [0000-0001-9316-7245](https://orcid.org/0000-0001-9316-7245)

References

- [1] Schütt K T, Sauceda H E, Kindermans P J, Tkatchenko A and Müller K R 2018 *The Journal of Chemical Physics* **148** 241722
- [2] Unke O T and Meuwly M 2019 *Journal of chemical theory and computation* **15** 3678–3693
- [3] Thölke P and De Fabritiis G 2022 *arXiv preprint arXiv:2202.02541*
- [4] Klicpera J, Groß J and Günnemann S 2020 *arXiv preprint arXiv:2003.03123*
- [5] Xie T and Grossman J C 2018 *Physical review letters* **120** 145301
- [6] Liu M, Luo Y, Wang L, Xie Y, Yuan H, Gui S, Yu H, Xu Z, Zhang J, Liu Y, Yan K, Liu H, Fu C, Oztekin B M, Zhang X and Ji S 2021 *Journal of Machine Learning Research* **22** 1–9 URL <http://jmlr.org/papers/v22/21-0343.html>
- [7] Fung V, Zhang J, Juarez E and Sumpter B G 2021 *npj Computational Materials* **7** 1–8
- [8] Ravi N, Chaturvedi P, Huerta E A, Liu Z, Chard R, Scourtas A, Schmidt K J, Chard K, Blaiszik B and Foster I 2022 *Scientific Data* **9** 657 ISSN 2052-4463 URL <https://doi.org/10.1038/s41597-022-01712-9>
- [9] Huerta E A, Khan A, Davis E, Bushell C, Gropp W D, Katz D S, Kindratenko V, Koric S, Kramer W T C, McGinty B, McHenry K and Saxton A 2020 *Journal of Big Data* **7** 88 (Preprint 2003.08394)
- [10] Huerta E A, Khan A, Huang X, Tian M, Levental M, Chard R, Wei W, Heflin M, Katz D S, Kindratenko V, Mu D, Blaiszik B and Foster I 2021 *Nature Astronomy* **5** 1062–1068 (Preprint 2012.08545)
- [11] Balaprakash P, Salim M, Uram T D, Vishwanath V and Wild S M 2018 Deephyper: Asynchronous hyperparameter search for deep neural networks 2018 *IEEE 25th international conference on high performance computing (HiPC)* (IEEE) pp 42–51
- [12] Ruddigkeit L, Van Deursen R, Blum L C and Reymond J L 2012 *Journal of chemical information and modeling* **52** 2864–2875
- [13] Wilmer C E, Farha O K, Bae Y S, Hupp J T and Snurr R Q 2012 *Energy & Environmental Science* **5** 9849–9856
- [14] Chmiela S, Tkatchenko A, Sauceda H E, Poltavsky I, Schütt K T and Müller K R 2017 *Science advances* **3** e1603015
- [15] Biewald L 2020 Experiment tracking with weights and biases software available from wandb.com URL <https://www.wandb.com/>
- [16] Gasteiger J, Becker F and Günnemann S 2021 *Advances in Neural Information Processing Systems* **34** 6790–6802
- [17] Choudhary K and DeCost B 2021 *npj Computational Materials* **7** 1–8
- [18] Chen C, Ye W, Zuo Y, Zheng C and Ong S P 2019 *Chemistry of Materials* **31** 3564–3572
- [19] Larsen A H, Mortensen J J, Blomqvist J, Castelli I E, Christensen R, Dułak M, Friis J, Groves M N, Hammer B, Hargus C *et al.* 2017 *Journal of Physics: Condensed Matter* **29** 273002
- [20] Wang M, Zheng D, Ye Z, Gan Q, Li M, Song X, Zhou J, Ma C, Yu L, Gai Y *et al.* 2019 *arXiv preprint arXiv:1909.01315*
- [21] Fey M and Lenssen J E 2019 Fast graph representation learning with PyTorch Geometric *ICLR Workshop on Representation Learning on Graphs and Manifolds*

- [22] Leow Y Y, Laurent T and Bresson X 2019 Graphtsne: A visualization technique for graph-structured data *ICLR Workshop on Representation Learning on Graphs and Manifolds*
- [23] Gelman S, Fahlberg S A, Heinzelman P, Romero P A and Gitter A 2021 *Proceedings of the National Academy of Sciences* **118** e2104878118
- [24] Mnih V, Kavukcuoglu K, Silver D, Rusu A A, Veness J, Bellemare M G, Graves A, Riedmiller M, Fidjeland A K, Ostrovski G *et al.* 2015 *nature* **518** 529–533
- [25] Pope P E, Kolouri S, Rostami M, Martin C E and Hoffmann H 2019 Explainability methods for graph convolutional neural networks *Proceedings of the IEEE/CVF Conference on Computer Vision and Pattern Recognition* pp 10772–10781
- [26] Papers with Code - Gradient Clipping Explained <https://paperswithcode.com/method/gradient-clipping> [Online; accessed 2022-11-21]
- [27] Glavatskikh M, Leguy J, Hunault G, Cauchy T and Da Mota B 2019 *Journal of cheminformatics* **11** 1–15
- [28] Bucior B J, Rosen A S, Haranczyk M, Yao Z, Ziebel M E, Farha O K, Hupp J T, Siepmann J I, Aspuru-Guzik A and Snurr R Q 2019 *Crystal Growth & Design* **19** 6682–6697
- [29] Choudhary K, Yildirim T, Siderius D W, Kusne A G, McDannald A and Ortiz-Montalvo D L 2022 *Computational Materials Science* **210** 111388
- [30] Krishnapriyan A S, Montoya J, Haranczyk M, Hummelshøj J and Morozov D 2021 *Scientific reports* **11** 1–11
- [31] Burner J, Schwiedrzik L, Krykunov M, Luo J, Boyd P G and Woo T K 2020 *The Journal of Physical Chemistry C* **124** 27996–28005
- [32] Moosavi S M, Novotny B Á, Ongari D, Moubarak E, Asgari M, Kadioglu Ö, Charalambous C, Guerrero A, Farmahini A H, Sarkisov L *et al.* 2022
- [33] Jolliffe I T and Cadima J 2016 *Philosophical Transactions of the Royal Society A: Mathematical, Physical and Engineering Sciences* **374** 20150202
- [34] Van der Maaten L and Hinton G 2008 *Journal of machine learning research* **9**
- [35] Wang Y, Huang H, Rudin C and Shaposhnik Y 2021 *J. Mach. Learn. Res.* **22** 1–73
- [36] Peltason L and Bajorath J 2007 *Journal of medicinal chemistry* **50** 5571–5578
- [37] Guha R and Van Drie J H 2008 *Journal of chemical information and modeling* **48** 646–658
- [38] Golbraikh A, Muratov E, Fourches D and Tropsha A 2014 *Journal of chemical information and modeling* **54** 1–4
- [39] Aldeghi M, Graff D E, Frey N, Morrone J A, Pyzer-Knapp E O, Jordan K E and Coley C W 2022 *Journal of Chemical Information and Modeling* **62** 4660–4671
- [40] Wilkinson M D, Sansone S A, Schultes E, Doorn P, da Silva Santos L O B and Dumontier M 2018 *Scientific Data* **5** 180118 URL <https://doi.org/10.1038/sdata.2018.118>
- [41] Wilkinson M D, Dumontier M, Aalbersberg I J, Appleton G, Axton M, Baak A, Blomberg N, Boiten J W, da Silva Santos L B, Bourne P E, Bouwman J, Brookes A J, Clark T, Crosas M, Dillo I, Dumon O, Edmunds S, Evelo C T, Finkers R, Gonzalez-Beltran A, Gray A J G, Groth P, Goble C, Grethe J S, Heringa J, 't Hoen P A C, Hooft R, Kuhn T, Kok R, Kok J, Lusher S J, Martone M E, Mons A, Packer A L, Persson B, Rocca-Serra P, Roos M, van Schaik R, Sansone S A, Schultes E, Sengstag T, Slater T, Strawn G, Swertz M A, Thompson M, van der Lei J, van Mulligen E, Velterop J, Waagmeester A, Wittenburg P, Wolstencroft K, Zhao J and Mons B 2016 *Sci. Data* **3** 160018
- [42] Chen Y, Huerta E A, Duarte J, Harris P, Katz D S, Neubauer M S, Diaz D, Mokhtar F, Kansal R, Park S E, Kindratenko V V, Zhao Z and Rusack R 2022 *Scientific Data* **9** 31 (Preprint [2108.02214](https://doi.org/10.1038/s41598-022-11081-1))
- [43] Barker M, Chue Hong N, Katz D S, Lamprecht A L, Martinez Ortiz C, Psomopoulos F, Harrow J, Castro L, Gruenpeter M, Martinez P and Honeyman T 2022 *Scientific Data* **9**
- [44] Duarte J, Li H, Roy A, Zhu R, Huerta E A, Diaz D, Harris P, Kansal R, Katz D S, Kavoori I H, Kindratenko V V, Mokhtar F, Neubauer M S, Eon Park S, Quinnan M, Rusack R and Zhao Z 2022 *arXiv e-prints* arXiv:2212.05081 (Preprint [2212.05081](https://arxiv.org/abs/2212.05081))

- [45] Park, Hyun and Zhu, Ruijie and Huerta, EA 2022 PhysNet for molecular dynamics applications in leadership class supercomputers. The Data and Learning Hub for Science <https://doi.org/10.26311/b6x8-4621>
- [46] Park, Hyun and Zhu, Ruijie and Huerta, EA 2022 MPNN_transformer for molecular dynamics applications in leadership class supercomputers. The Data and Learning Hub for Science <https://doi.org/10.26311/3pm2-am44>
- [47] Chard R, Li Z, Chard K, Ward L, Babuji Y, Woodard A, Tuecke S, Blaiszik B, Franklin M J and Foster I 2019 DLHub: Model and data serving for science *2019 IEEE International Parallel and Distributed Processing Symposium (IPDPS)* pp 283–292
- [48] Li Z, Chard R, Ward L, Chard K, Skluzacek T J, Babuji Y, Woodard A, Tuecke S, Blaiszik B, Franklin M J and Foster I 2021 *J. Parallel. Distrib. Comput.* **147** 64 ISSN 0743-7315

Appendix A. Hyperparameter tuning results of PhysNet with HOMO as target property

Table A1. Top 10 DeepHyper hyperparameter combinations for PhysNet with HOMO as target property.

agb	amp	batch_size	gradient_clip
3	TRUE	235	1.36E-01
1	TRUE	349	1.10E+00
14	FALSE	130	5.40E-05
3	FALSE	159	1.79E-02
5	TRUE	404	8.24E-02
4	TRUE	460	7.21E-02
13	TRUE	160	3.42E-05
4	FALSE	147	6.16E-02
7	TRUE	163	1.90E-01
1	TRUE	258	3.58E-02

Table A2. As Table A1 for the rest of parameters optimized through DeepHyper.

learning_rate	optimizer	weight_decay	objective
1.15E-03	sgd	2.94E-05	-1.604
8.69E-04	sgd	2.30E-06	-2.454
1.49E-04	lamb	1.17E-03	-2.976
5.64E-01	lamb	2.09E-04	-3.323
1.38E-03	sgd	4.83E-05	-6.474
2.33E-02	sgd	2.84E-04	-7.214
4.61E-04	lamb	1.74E-04	-12.494
5.99E-04	torch adamw	1.59E-03	-14.5111
5.26E-01	lamb	1.44E-04	-18.0449
6.95E-01	lamb	8.62E-05	-29.505

Appendix B. Examples of model explainability features

We present results to complement the interpretable AI analysis presented in Section 4.5. Figure B1 illustrates what information AI models may extract from input data to make predictions that are consistent with state-of-the-art knowledge on QM properties.

Appendix B.1. Grad-CAM interpretation

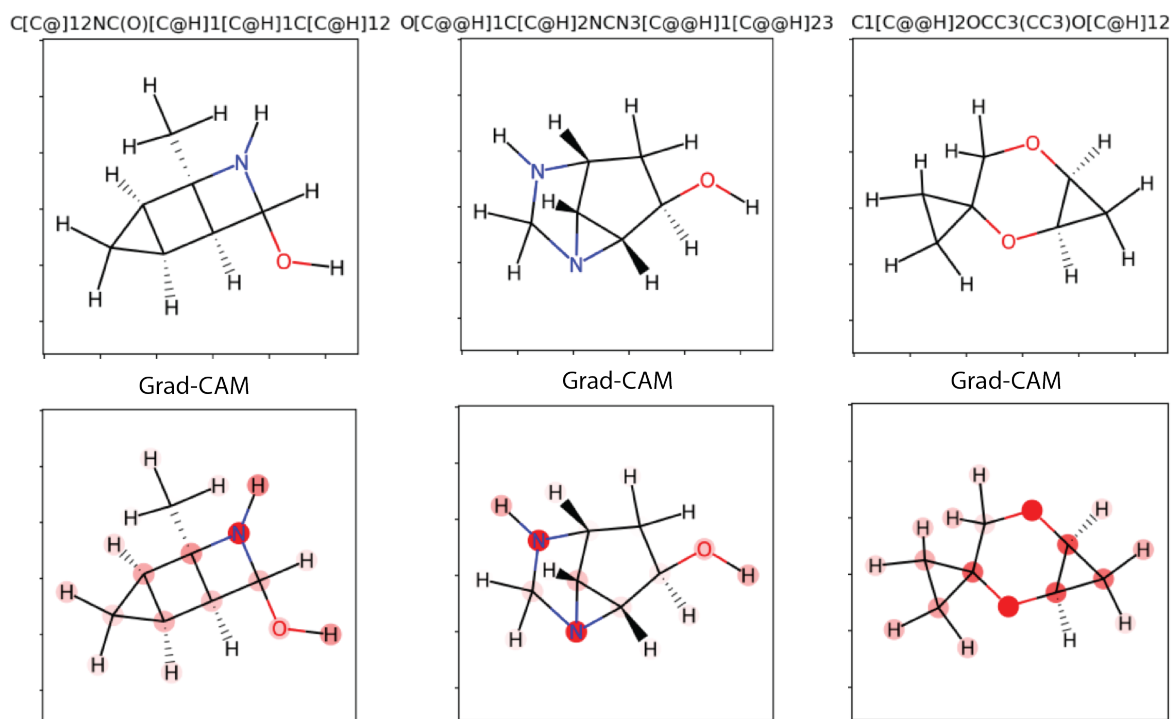


Figure B1. Molecular graphs (top) and Grad-CAM interpretations (bottom) of PhysNet with HOMO as target property for three example molecules. The N atoms and the H atoms attached to them are highlighted in red, indicating their higher weight in model predictions.

Appendix B.2. UMAP interpretation

Figure B2 shows that we can turn our AI predictors into feature extractors to explore clustering of molecules with similar properties.

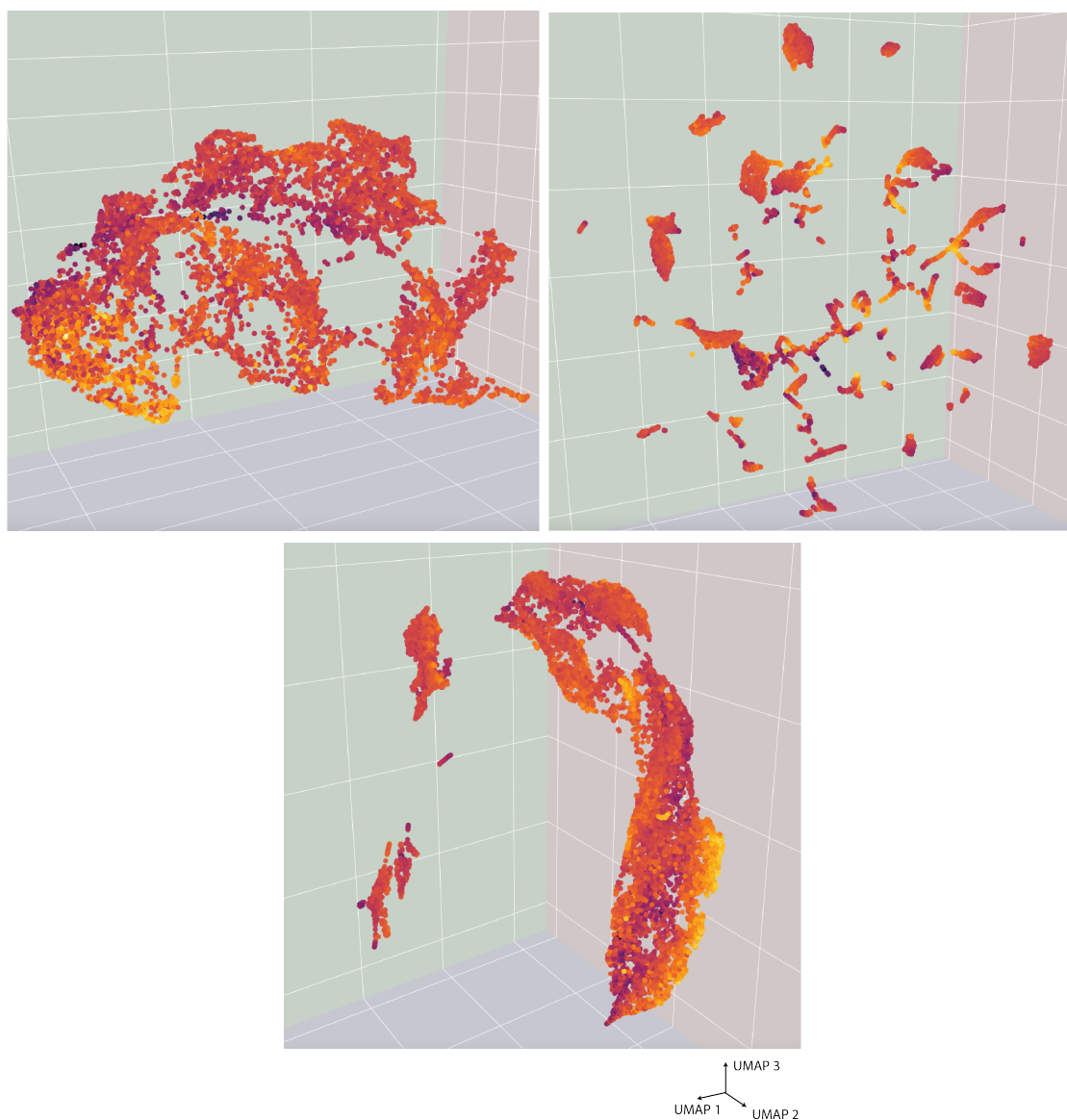


Figure B2. UMAP dimension reduction results for SchNet (top left), MPNN (top right) and MPNN-transformer (bottom) with HOMO as target property. A randomly selected 10% subset (13.4k molecules) of the QM9 dataset was used for analysis, which consists of stable small organic molecules composed of CHONF.